IEEE Access
Multidisciplinary | Rapid Review | Open Access Journal

Received June 15, 2020, accepted July 18, 2020, date of publication July 23, 2020, date of current version August 4, 2020.

Digital Object Identifier 10.1109/ACCESS.2020.3011524

Shape Synchronization in Driver-Response of 4-D Chaotic System and Its Application in Image Encryption

YUANYUAN HUANG[1], LONGWANG HUANG[2], YINHE WANG[3], YUXU PENG[1], AND FEI YU[1]

[1]College of Computer and Communication Engineering, Changsha University of Science and Technology, Changsha 410016, China
[2]School of Automation Science and Engineering, South China University of Technology, Guangzhou 510641, China
[3]School of Automation, Guangdong University of Technology, Guangzhou 510006, China

Corresponding author: Longwang Huang (longwang_huang@126.com)

This work was supported in part by the Science and Research Fund of Hunan Province Education Department under Grant 19C0083, in part by the Young Teacher Development Program Project of Changsha University of Science and Technology under Grant 2019QJCZ013 and Grant 2019QJCZ014, in part by the National Natural Science Foundation of China under Grant 61504013, and in part by the Natural Science Foundation of Hunan Province under Grant 2019JJ50648.

ABSTRACT In this paper, we put forward on the drive-response synchronization in shape for four-dimensional (4-D) continuous chaotic system, using the basic theory of plane curves in classical differential geometry. For 4-D continuous system, shape synchronization means the six-response systems have the same shape of chaotic attractor as the six projective systems of driver system. Numerical simulations are given to verify the theoretical analysis, which clearly shows that the shape controllers can really make two systems achieve shape synchronization in a quite short time. Moreover, a shape synchronization encryption algorithm for color image is proposed. Simulation results reveal the superiority of the proposed approach.

INDEX TERMS Shape synchronization, 4-D chaotic system, drive and response, chaotic attractor, image encryption.

I. INTRODUCTION

With the development of computer, communication, and network technologies, information security issues have attracted more and more attention and become a current research hotspot [1]–[6]. Chaos has characteristics such as unpredictability, pseudo-randomness, and extreme sensitivity to initial value [7], [8], it has been widely used in complex networks [9]–[13], memristors [14]–[19], random number generators [20], [21], secrecy communication technologies [22]–[25], especially the image encryption [26]–[29]. In information subject, chaos can be divided into two categories. One is to construct a new digital encryption algorithm using a chaotic system based on the computer finite precision technology. Zhou *et al.* proposed [30] a framework for parallel image encryption based on discretized chaotic map. Zhang *et al.* [31] proposed an image encryption algorithm based on the spatiotemporal chaos of the mixed linear-nonlinear coupled map lattices. An Efficient Image Encryption Scheme Based on S-Boxes and Fractional-Order Differential Logistic Map has been proposed in [32]. Based on matrix semi-tensor product theory, an algorithm for synchronously updating Boolean network encryption was proposed in [33]. Beyond that, some chaotic image encryption schemes using one-time keys [34], dynamic random growth technique [35], spatial bit-level permutation [36], genetic algorithm [37] and DNA rules [38]–[40] have been proposed. The other one is the chaotic secure communication system with chaotic synchronization as the technical core. Wang *et al.* [41] presented a new image encryption scheme based on time-delay Lorenz system synchronization. Vaidyanathan *et al.* [42] introduced a image encryption based on chaotic hyperjerk synchronization using an adaptive backstepping controller. Muthukumar *et al.* [43] designed an image encryption and decryption based on the synchronized lowest fractional order chaotic systems. Muthukumar *et al.* [44] proposed a new image encryption method of fast projective synchronization of fractional order dynamical systems. Therefore, many researchers have focused on chaotic synchronization and their synchronization techniques.

The associate editor coordinating the review of this manuscript and approving it for publication was Ilsun You.

Since Ott, Grebogi and York first observed chaos [45], and Pecora and Carroll first presented chaos synchronization [46] in 1990, two of the main concerns are their control and synchronization.Control refers to the adaptive control of a given chaotic system with the aim of forcing its states to be asymptotically stable, usually converging towards zero. Till, extensive researches have been devoted to various control strategies have been utilized such as active-passive control [47], [48], state feedback control [49]–[53], fuzzy model control [54], impulsive control [55], sliding mode control [56], [57] and adaptive control [58]–[60]. These methods can effectively solve the chaos control and chaos synchronization problems.

Various concepts of chaotic synchronization have been proposed, such as complete synchronization [61], [62], lag synchronization [63], projective synchronization [64], [65], phase synchronization [66], partial synchronization [67], general synchronization [68], anti-synchronization [69], [70]. These concepts of chaotic synchronization almost focus on state variables of drive and response systems. For completely synchronization, its states of the drive and the response system can be asymptotically stable, converging towards zero. In case of projective synchronization, its states of the drive and the response system can be synchronized up to a scaling factor. As well known, chaotic attractors can be described by smooth and continuous curve in some bounded region in with given initial condition for continuous chaotic systems. The chaotic attractors with different positions in phase space show the same or different shapes. According to the differential geometry theory of plane curve, two plane curves share the same shape when their signed curvature is equivalent while choosing the same arc-length parameter. In phase space, how to define the synchronization of two chaotic systems with the same shape of chaotic attractor with different positions? Therefore, if we pay attention to the shape of the drive chaotic attractor and control scheme, then a new problem for drive-response synchronization may be proposed.

In our previous work [71], [72], we proposed shape synchronization for a class of two-dimensional and three-dimensional chaotic systems and their application in secure communication system. Moreover, many classical hyper-chaotic systems have been proposed, such as hyper-chaotic Chen system [51], hyper-chaotic L$\ddot{u}$ system [73], hyper-chaotic Lorenz system [74] and Chua's chaotic system [75], [76]. Unlike two and three dimensional chaotic systems, the dynamics of higher dimensional chaotic systems is more complex and the shape of the chaotic attractors is invisible. It means that the shape of the higher chaotic attractors cannot be described by a single physical quality. On the other hand, in information transmission, higher dimension means stronger information carrying capacity. Therefore, it is very necessary to study the shape synchronization problem of higher dimensional chaotic systems.

Motivated by the above discussions, in this paper, shape synchronization of a class of continue 4-D chaotic system is discussed. The main the major advantages can be summarized as follows: (1) The shape synchronization schema for 4-D chaotic system is discussed. Compared with other chaotic synchronization, this kind of synchronization focus the shape of chaotic attractor instead of the distances between state variables of the drive and response systems, and means the six-response systems have the same shape of chaotic attractor as the six projective systems of drive system. However, there are no further studies about this work. (2) By getting the purpose of control, the group of shape controllers are designed based on the classical differential geometry technique. Under these controllers, the chaotic attractor of response system and drive system have the same arc length measure and relative curvature,and two systems achieve shape synchronization in a short time. The synchronization error and timing is investigated. (3) A lightweight image encryption algorithm by using shape synchronization is proposed. The senders uses the 4-D chaotic system to encrypt the image file, and sends the driving signal and Key to the receiver. As this time, the shape controller is used to synchronize the response system in shape, then decrypted the inverse operation of the encryption algorithm to obtain the decrypted image file. During this period, the scheme used the shape characteristics variables of drive system as the driving signals. So, the attackers are hard to identify the type of chaotic system using these driving signals. Even if the worse-case scenario attackers are able to successfully access these driving signals and only possible to plot the shape of driving chaotic attractor rather than the accurate position. On the other side, the proposed scheme can achieve fast synchronization in shape, which can also enhance the synchronization rate and is suitable for real-time communication system.

The rest of this paper is organized as follows. Section II presents the basic concepts of classical differential geometry. Section III describes the shape synchronization model of 4-D chaotic system. Section IV is about the definition of shape synchronization and the design of shape controller. The reconstruction process of the chaotic drive system and the numerical simulations shown in section V. An image encryption algorithm based on the shape synchronization is proposed in section VI. Conclusions are drown in the last section.

II. PRIORI KNOWLEDGE OF PLANE CURVE

Let $r = r(t) \in R^n$, $t \in R^+$, $R^+ \in [0, +\infty)$ be a regular curve in R^n. It is a plane curve when $n = 2$ and when $n = 3$, it is a spacial curve. ''regular'' means to any $t \in R^+$, $r'(t) = dr(t)/dt$ does not vanish. By the way, all the curves mentioned in this paper are regular curves.

The arc-length parameter s of curve $r = r(t)$ is defined by the equation $s(t) = \int_{t_0}^{t_1} \|r'(\tau)\| d\tau$, which indicates the unit length of the curve between the point $r(t_0)$ and $r(t_1)$. Obviously, for any $t \in R^+$, $s'(t) > 0$, there must be an anti-function $t = t(s)$.

Consider the plane curve $r(t) = (x(t), y(t))^T \in R^2$ on the Cartesian right hand Frame. The unit tangent is defined as:

$$T(t) = \frac{r'(t)}{|r'(r)|} = \frac{1}{\sqrt{(x'(t))^2 + (y'(t))^2}} \begin{bmatrix} x'(t) \\ y'(t) \end{bmatrix} \quad (1)$$

The unit normal vector is defined as:

$$N(t) = \frac{1}{\sqrt{(x'(t))^2 + (y'(t))^2}} \begin{bmatrix} -y'(t) \\ x'(t) \end{bmatrix} \tag{2}$$

It is easy to figure out that $\|T(t)\| = 1, \|N(t)\| = 1, (T(y), N(t)) = 0, t \in R^+$. $\| * \|$ denotes Euclidean norm, $(*)$ denotes the inner product. The signed curvature $\rho(t)$ is defined as.

$$\rho(t) = \frac{x'(t)y''(t) - x''(t)y'(t)}{[(x'(t))^2 + (y'(t))^2]^{3/2}} \tag{3}$$

Extraordinarily, if we choose the arc-length s as the parameter instead of time t, the relationship between the signed curvature $\rho(s)$, unit tangent vector $T(s)$ and unit normal vector $N(s)$ can be described by.

$$\dot{T}(s) = \rho(s)N(s), \quad \dot{N}(s) = -\rho(s)T(s) \tag{4}$$

It is called Frenet-Serret formula. Meanwhile, we have the signed curvature $\rho(s)$, unit tangent $T(s)$ and unit normal vector $N(s)$ as below.

$$\begin{aligned} \rho(s) &= \dot{x}(s)\ddot{y}(s) - \ddot{x}(s)\dot{y}(s) \\ T(s) = \dot{r}(s) &= \begin{bmatrix} \dot{x}(x) \\ \dot{y}(s) \end{bmatrix}, \quad N(s) = \begin{bmatrix} -\dot{y}(s) \\ \dot{x}(s) \end{bmatrix} \end{aligned} \tag{5}$$

Suppose there are two arc-length parameterized regular curve $r_1(s)$ and $r_2(s)$. If their signed curvature $\rho_1(s)$ and $\rho_2(s)$ are equivalent everywhere and do not vanish, then the curve $r_1(s)$ and $r_2(s)$ can be transformed to each other by a rotation and a translation. It means that $r_1(s) = Ar_2(s) + \Upsilon_0$,

$$A = \begin{bmatrix} cos\theta_0 & -sin\theta_0 \\ sin\theta_0 & cos\theta_0 \end{bmatrix}, \quad \Upsilon_0 = \begin{bmatrix} x_0 \\ y_0 \end{bmatrix}$$

in which θ_0 is the rotation angle, and Υ_0 is the translation vector.

Definition 1: Consider two t-parameterized regular plane curve $r_1(t)$ and $r_2(t)$. Make arc-length s be the common parameter from initial time t_0. If there exist a matrix $A = [cos\theta_0, -sin\theta_0; sin\theta_0, cos\theta_0]$ and a vector $\Upsilon_0 = [x_0, y_0]^T$ such that $r_1(s) = Ar_2(s) + \Upsilon_0$, then the two plane curve $r_1 = r_1(t)$ and $r_2 = r_2(t)$ are called to share the same shape.

III. SHAPE SYNCHRONIZATION SCHEME

A. DESCRIPTION OF DRIVE SYSTEM

Consider the following four-dimensional chaotic systems.

$$\begin{cases} \dot{x_1} = f_1(x, t) \\ \dot{x_2} = f_2(x, t) \\ \dot{x_3} = f_3(x, t) \\ \dot{x_4} = f_4(x, t) \end{cases} \tag{6}$$

where $x = [x_1, x_2, x_3, x_4]^T \in R^4$ is the state vector of the system and $f_i (i = 1, 2, 3, 4)$ is a smooth nonlinear function.

Remark 1: Many four-dimensional chaotic systems can be described by the Eq. (6), such as hyper-lorenz, hyper-chen, hyper-zhou, etc. This implies that model (6) has the common feature of four-dimensional chaotic systems.

Under a given initial condition, the chaotic attractor of the system described by Eq. (6) is a regular four-dimensional spacial curve. Referring to paper [77], [78], the geometry theory of plane curve can be utilized by projecting the chaotic attractor onto the coordinate planes. When t_0 and $x_0 = (x_1(t_0), x_2(t_0), x_3(t_0), x_4(t_0))^T$ are given, the solutions of the Eq. (6) are: $x_1(t) = \vartheta_1(x_0, t_0, t) \triangleq \xi_1(t)$, $x_2(t) = \vartheta_2(x_0, t_0, t) \triangleq \xi_2(t)$, $x_3(t) = \vartheta_3(x_0, t_0, t) \triangleq \xi_3(t)$, $x_4(t) = \vartheta_4(x_0, t_0, t) \triangleq \xi_4(t)$.

Obviously, $\xi = \xi(t) = (\xi_1(t), \xi_2(t), \xi_3(t), \xi_4(t)) \in R^4$ is a state trajectory of the system (6). Let the coordinate axes be x_1, x_2, x_3, x_4, the coordinate origin is O. By projecting the trajectory $\xi = \xi(t)$ onto the coordinate planes x_1ox_2, x_1ox_3, x_1ox_4, x_2ox_3, x_2ox_4, x_3ox_4 respectively, the following projective system can be obtained.

$$\begin{cases} \dot{x}_i = f_i(x_i, x_j, \xi_a(t), \xi_b(t), t) \\ \dot{x}_j = f_j(x_i, x_j, \xi_a(t), \xi_b(t), t) \end{cases} \tag{7}$$

where $i, j, a, b \in \{1, 2, 3, 4\}$ satisfying that $i < j, a \neq b$ and $a, b \in \{1, 2, 3, 4\} - \{i, j\}$. The projective system describes the project curves of the chaotic attractor of drive system (6).

Definition 2: System (7) is called as the projective system of drive system (6). The projective system consists of six subsystems. When $i = 1, j = 2, a = 3, b = 4$, the corresponding projective subsystem is abbreviated as $DS - I$; When $i = 1, j = 3, a = 2, b = 4$, the corresponding projective subsystem is abbreviated as $DS - II$; when $i = 1, j = 4, a = 2, b = 3$,the corresponding projective subsystem is abbreviated as $DS - III$; When $i = 2, j = 3, a = 1, b = 4$,the corresponding projective subsystem is abbreviated as $DS - IV$; When $i = 2, j = 4, a = 1, b = 3$, the corresponding projective subsystem is abbreviated as $DS - V$; When $i = 3, j = 4, a = 1, b = 1$, the corresponding projective subsystem is abbreviated as $DS - VI$.

B. DESCRIPTION OF RESPONSE SYSTEM

Consider the projective system (7), the corresponding controlled response system is designed as.

$$\begin{cases} \dot{y}_1^k = \alpha_1^k(y^k, t)u_1^k(t) \\ \dot{y}_2^k = \alpha_2^k(y^k, t)u_1^k(t) \\ \dot{y}_3^k = \beta(y^k, t) + \alpha_3^k(y^k, t)u_1^k(t) + \omega^k(y^k, t)u_2^k(t) \end{cases} \tag{8}$$

The response system is also made up of six subsystems which are abbreviated as $RS - k$ and $k = I, II, III, IV, V, VI$. $y^k = (y_1^k, y_2^k, y_3^k)^T \in R^3$ is the state vector, $\alpha^k(y^k, t)$, $\beta^k(y^k, t)$, $\omega^k(y^k, t)$ are derivable time varying functions and $u^k(t) = (u_1^k(t), u_2^k(t))^T$ is the control input.

If given the initial state $y_0^k = y^k(t_0)$, starting time t_0 and control input $u^k(t)$, then the plane curve determined by the first two equations of Eq. (8) can be described as $\tilde{r}^k = (y_1^k(t), y_2^k(t))^T$.

Definition 3: Plane curve $\tilde{r}^k = (y_1^k(t), y_2^k(t))^T$ is called as the project curve of $RS - k$ which is described by Eq. (8). Abbreviated as $PCR - k, k = I, II, III, IV, V, VI$. (The

meaning of the symbols that mentioned in Definition 2 and Definition 3 is shown is Table 1).

TABLE 1. Symbols mentioned in Definition 2.

Plane	subsystem of system (7)	
x_1ox_2	$DS-I,$	$i=1,j=2,a=3,b=4$
x_1ox_3	$DS-II,$	$i=1,j=3,a=2,b=4$
x_1ox_4	$DS-III,$	$i=1,j=4,a=2,b=3$
x_2ox_3	$DS-IV,$	$i=2,j=3,a=1,b=4$
x_2ox_4	$DS-V,$	$i=2,j=4,a=1,b=3$
x_3ox_4	$DS-VI,$	$i=3,j=4,a=1,b=2$

IV. SHAPE SYNCHRONIZATION AND CONTROL OF CHAOS

A. DEFINITION OF SHAPE SYNCHRONIZATION

Definition 4: Consider the drive system (6) and response system (8), if the plane curve $PCR-k$ which is the defined by response subsystem $RS-k$ shares the same shape with the plane curve that defined by projective subsystem $DS-k$, then $RS-k$ is called as shape synchronized with system $DS-k$. If to all $k=I,II,III,IV,V,VI$ that $RS-k$ is shape synchronized with $DS-k$, then we call that the response system (8) is synchronized with drive system (6) in shape.

Definition 5: If there exist a group of controller $u^k(t)=(u_1^k(t),u_2^k(t))^T$, $k=I,II,III,IV,V,VI$, under the control of which, response system(8) is shape synchronized with drive system(6), then $u^k(t)=(u_1^k(t),u_2^k(t))^T$, $k=I,II,III,IV,V,VI$ is called as a group of shape synchronization controllers.

B. SHAPE SYNCHRONIZATION CONTROLLER DESIGN

The main usage of the shape synchronization controller $u^k(t)=(u_1^k(t),u_2^k(t))^T$ is to guarantee that the plane curve $PCR-k$ shares the same shape with the plane curve that determined by the projective subsystem $DS-k$. According to the differential geometry theory of plane curve, if two plane curves share the same shape, their arc-length parameterized signed curvature must be equivalent everywhere. Therefore, the designing procedure of the shape synchronization controller can be divided into two steps.

step 1: Design controller $u_1^k(t)$ which make sure that the plane curve $PCR-k$ and the plane curve that determined by projective system $DS-k$ have the same arc-length parameter.

step 2: Design controller $u_2^k(t)$ which ensure that the signed curvature of $PCR-k$ and the signed curvature of the plane curve determined by projective system $DS-k$ are equivalent everywhere. The following assumptions are propose.

Assumption 1: Consider the response system (8), the following inequality is true for any $t\in[t_0,\infty)$, $k=I,II,III,IV,V,VI$, where $t_0\in R$ is the initial time.

$$(\alpha_1^k(y^k,t))^2+(\alpha_2^k(y^k,t))^2\neq 0 \tag{9}$$

Assumption 2: Consider the response system (8), the following inequality is true for any $t\in[t_0,\infty)$, $k=I,II,III,IV,V,VI$, where $t_0\in R$ is the initial time.

$$\{[\alpha_1^k(y^k,t),\alpha_2^k(y^k,t)](y_3^k)\}\omega^k(y^k,t)\neq 0 \tag{10}$$

where the *Lie-Bracket* is follow the form.

$$[\alpha_1^k(y^k,t),\alpha_2^k(y^k,t)](y_3^k)=\alpha_1^k(y^k,t)\frac{\delta\alpha_2^k(y^k,t)}{\delta y_3^k}-\alpha_2^k(y^k,t)\frac{\delta\alpha_1^k(y^k,t)}{\delta y_3^k}$$

Remark 2: The function of Assumption 1 is to make sure that the plane curve $PCR-k$ is regularly positive defined. Assumption 2 is utilized to synthesize the controller $u_2^k(t)$ which guarantee the equivalence of the signed curvature of $PCR-k$ and the curve determined by projective system $DS-k$.

According to Assumption 1 and Assumption 2, a group of shape synchronization controller is designed as follow.

Remark 3: For simplicity, parameters t in $u_1^k(t)$ and $u_2^k(t)$ has been omitted in this section.

$$\begin{aligned}u_1^k&=\sqrt{\frac{(f_i(x_i,y_i,\xi_a,\xi_b,t))^2+(f_j(x_i,y_i,\xi_a,\xi_b,t))^2}{(\alpha_1^k(y^k,t))^2+(\alpha_2^k(y^k,t))^2}}\\ u_2^k&=\frac{\rho_d^k[(f_i(x_i,y_i,\xi_a,\xi_b,t))^2+(f_j(x_i,y_i,\xi_a,\xi_b,t))^2]^{3/2}}{(u_1^k)^2\{[\alpha_1^k(y^k,t),\alpha_2^k(y^k,t)](y_3^k)\}\omega^k(y^k,t)}\\ &\quad-\frac{\sigma(y^k,t)}{(u_1^k)^2\{[\alpha_1^k(y^k,t),\alpha_2^k(y^k,t)](y_3^k)\}\omega^k(y^k,t)}\end{aligned} \tag{11}$$

in which

$$\begin{aligned}\psi=&\left\{(\alpha_1^k(y^k,t))^2\frac{\delta\alpha_2^k(y^k,t)}{\delta y_1^k}-(\alpha_2^k(y^k,t))^2\frac{\delta\alpha_1^k(y^k,t)}{\delta y_2^k}\right.\\ &\left.+\left[\frac{\delta\alpha_2^k(y^k,t)}{\delta y_2^k}-\frac{\delta\alpha_1^k(y^k,t)}{\delta y_1^k}\right]\alpha_1^k(y^k,t)\alpha_2^k(y^k,t)\right\}(u_1^k)^3,\\ \sigma(y^k,t)=&\left\{[\alpha_1^k(y^k,t),\alpha_2^k(y^k,t)](y_3^k)\right\}[\beta^k(y^k,t)\\ &+\alpha_3^k(y^k,t)u_1^k]+\psi.\end{aligned}$$

When given the initial state x_0 and time t_0, the signed curvature ρ_d^k can be calculated according to the following formula.

$$\rho_d^k=\frac{\dot{x}_i\ddot{x}_j-\ddot{x}_i\dot{x}_j}{[(f_i(x_i,y_i,\xi_a,\xi_b,t))^2+(f_j(x_i,y_i,\xi_a,\xi_b,t))^2]^{3/2}}$$

Theorem 1: If Assumption 1 is true, then under the control of $u_1^k(t)$, the signed curvature of $PCR-k$ possess the same arc-length measure as the plane curve defined by projective system $DS-k$.

Proof: According to Eq. (7), the arc-length s_d^k of the projective drive system $DS-k$ can be calculated as.

$$s_d^k=\int_{t_0}^{t}\sqrt{f_i(x_i,y_i,\xi_a,\xi_b,t))^2+(f_j(x_i,y_i,\xi_a,\xi_b,t))^2}dt \tag{12}$$

The arc-length s_r^k of plane curve $PCR-k$ can be calculated as.

$$s_r^k = \int_{t_0}^{t} \sqrt{(\dot{y}_1^k)^2 + (\dot{y}_2^k)^2}dt \tag{13}$$

■

Substituting the controller (11) into (13), then there exist $s_d^k - s_r^k = 0, k = I, II, III, IV, V, VI$. Theorem 1 is proved.

Theorem 2: If both Assumption 1 and Assumption 2 are true, under the control of u_1^k, u_2^k, the signed curvature of the plane curve $PCR-k$ and the curve determined by projective system $DS-k$ is equivalent everywhere.

Proof: Referring to Eq. (3), the signed curvature ρ_d^k of the curve determined by projective system $DS-k$ can be calculated as follows.

$$\rho_d^k = \frac{\dot{x}_i\ddot{x}_j - \ddot{x}_i\dot{x}_j}{[f_i^2(x_i, y_i, \xi_a, \xi_b, t) + f_j^2(x_i, y_i, \xi_a, \xi_b, t)]^{3/2}} \tag{14}$$

Similarly, the curvature ρ_r^k of $PCR-k$ is.

$$\rho_r^k = \frac{\dot{y}_1^k\ddot{y}_2^k - \ddot{y}_1^k\dot{y}_2^k}{[(\alpha_1^k(y^k, t)u_1^k)^2 + (\alpha_2^k(y^k, t)u_1^k)^2]^{3/2}} \tag{15}$$

On the basis of Assumption 1 and Assumption 2, it is easy to figure out that.

$$\begin{aligned}
&\dot{y}_1^k\ddot{y}_2^k - \ddot{y}_1^k\dot{y}_2^k \\
&= \alpha_1^k u_1^k\left[\frac{d\alpha_2^k(y^k, t)}{dt}u_1^k - \alpha_2^k(y^k, t)\frac{du_1^k}{dt}\right] \\
&\quad - \alpha_2^k u_1^k\left[\frac{d\alpha_1^k(y^k, t)}{dt}u_1^k - \alpha_1^k(y^k, t)\frac{du_1^k}{dt}\right] \\
&= \left[\alpha_1^k(y^k, t)\frac{d\alpha_2^k(y^k, t)}{dt} - \alpha_2^k(y^k, t)\frac{d\alpha_1^k(y^k, t)}{dt}\right](u_1^k)^2 \\
&= \sigma(y^k, t)\{[\alpha_1^k(y^k, t), \alpha_2^k(y^k, t)](y_3^k)\}\omega^k(y^k, t)u_2^k,
\end{aligned} \tag{16}$$

By Substituting equation (16) into (15), the curvature of $PCR-k$ can be obtained as.

$$\begin{aligned}
\rho_r^k = &\frac{(u_1^k)^2\{[\alpha_1^k(y^k, t), \alpha_2^k(y^k, t)](y_3^k)\}\omega^k(y^k, t)u_2^k}{[(\alpha_1^k(y^k, t)u_1^k)^2 + (\alpha_2^k(y^k, t)u_1^k)^2]^{3/2}} \\
&+ \frac{\sigma(y^k, t)}{[(\alpha_1^k(y^k, t)u_1^k)^2 + (\alpha_2^k(y^k, t)u_1^k)^2]^{3/2}}
\end{aligned} \tag{17}$$

Replacing the $u_1^k(t), u_2^k(t)$ in Eq (17) with (11), then to all $k = I, II, III, IV, V, VI$, we have.

$$\rho_d^k - \rho_r^k = 0 \tag{18}$$

The proof of Theorem 2 completes. ■

Theorem 3: Consider the drive system (6), projective system (7) and response system (8), if both Assumption 1 and Assumption 2 are true, then under the effect of controller (11), the response system (8) is shape synchronized with the chaotic drive system (6).

Remark 4: Referring to Definition 4 and Theorem 3, that the response system (8) and chaotic drive system (6) achieved shape synchronization on the whole. It means that the trajectory whose projections on the two dimension coordinate planes are $PCR-k$ shares the same shape with the trajectory of the drive system (6). But,due to the position difference, their state is not completely the same. Theorem 3 does not explain how to reconstruct the the state of chaotic drive system (6) from the state of the response system (8) after chaotic shape synchronization is achieved. Actually, according to Theorem 3 and the conclusions of shape synchronization, it is definitely capable to reconstruct all the states of the drive system (6). The reconstruction of the states is performed in the next section.

V. RECONSTRUCT OF 4-D CHAOTIC SYSTEMS AND NUMERICAL SIMULATION

A. RECONSTRUCT SHAPE SYNCHRONIZATION OF 4-D CHAOTIC SYSTEMS

In this section, we are going to explain how to reconstruct the state of drive system (6) from the state of response system (8) on the basis of the Theorem 1- 3. Before that, let's review the following truth first.

Let $x_0 = (x_1(t_0), x_2(t_0), x_3(t_0), x_4(t_0))^T$ be the initial state of the drive system (6) at time t_0, using the symbols in subsection III-A, the state trajectory of system (6) is $\xi(t) = (\xi_1(t), \xi_2(t), \xi_3(t), \xi_4(t))^T \in R^4$. It's projection on the coordinate plane is described by Eq. (7), the unit tangent vector and unit normal vector of the plane curve $r^k = (x_i(t), x_j(t))$ at the initial point $r_0^k = (x_i(t_0), x_j(t_0))$ can be calculated as bellow.

$$\begin{aligned}
T_0^k &= \frac{1}{\sqrt{f_i^2(x_0, t_0) + f_j^2(x_0, t_0)}}\begin{bmatrix} f_i(x_0, t_0) \\ f_j(x_0, t_0) \end{bmatrix} \\
N_0^k &= \frac{1}{\sqrt{f_i^2(x_0, t_0) + f_j^2(x_0, t_0)}}\begin{bmatrix} -f_j(x_0, t_0) \\ f_i(x_0, t_0) \end{bmatrix}
\end{aligned} \tag{19}$$

where $k = I, II, III, IV, V, VI$, $i, j = 1, 2, 3, 4$, $i < j$. Table 2 presents the corresponding relationship between the projective curves, initial unit tangent vectors and normal vectors.

TABLE 2. Symbols mentioned in Definition 3.

subsystem of system (8)		Project curves	
$RS-I$,	$k=I$	$PCR-I$,	$\tilde{r}^I(t)$
$RS-II$,	$k=II$	$PCR-II$,	$\tilde{r}^{II}(t)$
$RS-III$,	$k=III$	$PCR-III$,	$\tilde{r}^{III}(t)$
$RS-IV$,	$k=IV$	$PCR-IV$,	$\tilde{r}^{IV}(t)$
$RS-V$,	$k=V$	$PCR-V$,	$\tilde{r}^{V}(t)$
$RS-VI$,	$k=VI$	$PCR-VI$,	$\tilde{r}^{VI}(t)$

Due to the Theorem 1-3, under the effect of controller of controller (11), the plane curve $PCR-k$ (parametric function $\tilde{r}^k = (y_1^k(t), y_2^k(t))^T$) that defined by response system $RS-k$ shares the same shape with the plane curve (parametric function $r^k = (x_i(t), x_j(t))^T$) defined by projective system $DS-k$. It means that signed curvature $\rho_d^k(s^k) = \rho_r^k(s^k)$ (arc-length parameter $s^k = s_d^k = s_r^k$). Therefore, according to Definition 1 and basic theory of plane curve. In the same coordinate

TABLE 3. Projections and initial vectors.

Coordinate plane	Projection	value of k	value of i, j	Initial vectors
x_1ox_2	r^I	$k = I$	$i = 1, j = 2$	T_0^I, N_0^I
x_1ox_3	r^{II}	$k = II$	$i = 1, j = 3$	T_0^{II}, N_0^{II}
x_1ox_4	r^{III}	$k = III$	$i = 1, j = 4$	T_0^{III}, N_0^{III}
x_2ox_3	r^{IV}	$k = IV$	$i = 2, j = 3$	T_0^{IV}, N_0^{IV}
x_2ox_4	r^V	$k = V$	$i = 2, j = 4$	T_0^V, N_0^V
x_3ox_4	r^{VI}	$k = VI$	$i = 3, j = 4$	T_0^{VI}, N_0^{VI}

system, Let $\tilde{T}_0^k, \tilde{N}_0^k$ be the unit tangent vector and the normal vector of the plane curve $PCR-k$ at the time t_0. If there are $\tilde{r}_0^k = r_0^k, \tilde{T}_0^k = T_0^k, \tilde{N}_0^k = N_0^k$, then the plane curve $PCR-k$ is completely coincident with the plane curve that determined by projective system $DS-k$. It is to say that the state of the system that corresponding to $PCR-k$ is exactly the same with the state of the projective drive system $DS-k$.

To summarize, if T_0^k, N_0^k represent the unit tangent vector and normal vector of the projective system $DS-k$ respectively, then the following differential equation can be obtained by utilizing the the radius vector of $PCR-k$, signed curvature $\rho_r^k(s^k)$ and the *Frenet-Serret* formula when given the initial state r_0, T_0^k, N_0^k.

$$\begin{cases} \dot{s}^k = \|\tilde{r}^k(t)\| \\ \dot{r}^k = T_d^k(s^k) \\ \dot{T}_d^k(s^k) = \rho_r^k(s^k) N_d^k(s^k) \\ \dot{N}_d^k(s^k) = -\rho_r^k(s^k) T_d^k(s^k) \\ \dot{y}_1^k = \alpha_1^k(y^k, t) u_1^k(t) \\ \dot{y}_2^k = \alpha_2^k(y^k, t) u_1^k(t) \\ \dot{y}_3^k = \beta^k(y^k, t) + \alpha_3^k(y^k, t) u_1^k(t) + \omega^k(y^k, t) u_2^k(t) \end{cases} \tag{20}$$

where initial state $s_0^k = s^k(t_0) = 0$, $y_3^k(t_0) = 0$, $r^k(t_0) = r_0^k$, $T_d^k(t_0) = T_0^k, N_d^k = N_0^k$. u_1^k, u_2^k are given by Eq.(11).

Let $r^k(t) = (\eta_1^k(t), \eta_2^k(t))^T$ be the solution of equation (20) under the above given initial condition. Referring to the symbols in Definition 2, the state of the chaotic drive system (6) can be reconstructed as follow.

$$\xi = \xi(t) = (\eta_1^I, \eta_2^I, \eta_1^{VI}, \eta_2^{VI})^T \tag{21}$$

Except (21), other similar results can be obtained as well. Such as,

$$\xi = \xi(t) = (\eta_1^I, \eta_1^{IV}, \eta_2^{II}, \eta_2^{III})^T,$$
$$\xi = \xi(t) = (\eta_1^{II}, \eta_1^V, \eta_2^{IV}, \eta_2^{VI})^T.$$

Theorem 4: Consider the four-dimensional chaotic drive system (6), if given the initial condition $s_0^k = s^k(t_0) = 0$, $y_3^k = 0$, $r^k(t_0) = r_0^k$, $T_s^k(t_0) = T_0^k$, $N - d^k(t_0) = N_0^k$, then under the effect of controller (11) response system (8) can make sure that the system (21) is the same with the drive system (6).

B. NUMERICAL SIMULATION

In this section, a numerical simulation will be conducted on a hyper-Lü system to illustrate and compare the control and synchronization results. The dynamic equation of the hyper-Lü is follow the form.

$$\begin{cases} \dot{x}_1 = a(x_2 - x_1) \\ \dot{x}_2 = cx_2 - x_1x_3 + x_4 \\ \dot{x}_3 = x_1x_2 - bx_3 \\ \dot{x}_4 = x_3 - dx_4 \end{cases} \tag{22}$$

where $a = 20$, $b = 5$, $c = 10$, $d = 1.5$. The projections on the coordinate planes of the chaotic attractor when given the initial state $x_1(0) = 1, x_2(0) = -2, x_3(0) = 3, x_4(0) = -9$ are shown in Fig. 1.

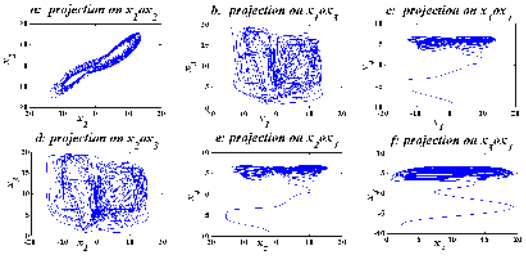

FIGURE 1. Projections of the drive system chaotic attractor.

According to Eq. (19), we can figure out the unit tangent vector and normal vector of the system's (22) project curves at the initial point.

$$\begin{aligned} T_d^I(0) &= [-0.8824, -0.4706]^T, \quad N_d^I = [0.4706, -0.8824]^T \\ T_d^{II}(0) &= [-9621, -0.2726]^T, \quad N_d^{II} = [0.2726, -9621]^T \\ T_d^{III}(0) &= [-0.9642, 0.2652]^T, \quad N_d^{III} = [-0.2652, -0.9642]^T \\ T_d^{IV}(0) &= [-1.3310, -0.7071]^T, \quad N_d^{IV} = [0.7071, -1.3310]^T \\ T_d^V(0) &= [-0.8888, 0.4583]^T, \quad N_d^V = [-0.4583, -0.8888]^T \\ T_d^{VI}(0) &= [-0.7176, 0.6965]^T, \quad N_d^{VI} = [-0.6965, -0.7176]^T \end{aligned} \tag{23}$$

Before reconstruct chaotic drive system, we need to reconstruct the project curves $r^k(t)$ of the drive system chaotic attractor. The project curve of the drive system (22) on the coordinate plane x_1ox_2 is $r^I(t) = (x_1(t), x_2(t))^T$. Referring to Eq. (8), the response subsystem can be designed as $\alpha_1^I(y^I, t) = sin(y_3^I)$, $\alpha_2^I(y^I, t) = cos(y_3^I)$, $\beta^I(y^I, t) = 0$, $\alpha_3^I(y^I, t) = 0$, $\omega^I(y^I, t) = 1$. Apparently $(\alpha_1^I(y^I, t))^2 + (\alpha_2^I(y^I, t))^2 \neq 0$, $\{[\alpha_1^I(y^I, t), \alpha_2^I(y^I, t)](y_3^I)\}\omega^I(y^I, t) \neq 0$, thus the response subsystem meets Assumption 1 and Assumption 2. According to (11), the author designed the following shape controller for the response subsystem:

$$\begin{aligned} u_1^I &= \sqrt{\dot{x}_1^2 + \dot{x}_2^2} \\ u_2^I &= \frac{\ddot{x}_1\dot{x}_2 - \ddot{x}_2\dot{x}_1}{(u_1^I)^2} \end{aligned} \tag{24}$$

The curve $r^I(t)$ can be reconstructed by solving the equation that follow the form of Eq. (20) ($k = 1$). The initial value of

the function is given bellow.

$$\begin{aligned} s^I(0) &= 0, \quad y_1^I(0) = -1, \\ y_2^I(0) &= 2, \quad y_3^I(0) = 0, \\ T_d^I &= [-8824, -0.4706]^T, \\ N_d^I &= [0.4706, -8824]^T, \end{aligned} \tag{25}$$

The figure (a)-(f) in Fig. 2 show the the project curves of the drive system (22), plane curves defined by response system and the reconstructed project curves of the drive system.

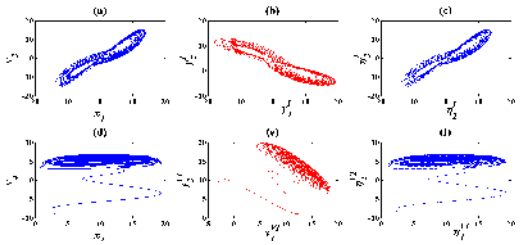

FIGURE 2. Project curves of drive system,response system and reconstructed system. (a) Project curve r^I; (b) Plane curve $\tilde{r}^I$; (c) Reconstructed curve r^I; (d) Project curve r^{VI}; (e) Plane curve $\tilde{r}^{VI}$; (f) Reconstructed curve r^{VI}.

From Fig. 2, it is easy to figure out that image (a) and (b) share the same geometry shape, so as image (d) and (e). It indicates that the project curves of drive system (22) share the same shape with the plane curves defined by response subsystem $RS-VI$. Although, the plane curves have identical geometry shape, but their position is not exactly the same. It is the reason why we need to reconstruct these plane curves. Image (c) and (f) in Fig. 2 display the plane curves that are reconstructed from the state of the response system. As we can see that the position of the curves in image (a) and (c) is totally the same, so as the curves in image (f) and (d). It implies that the state that these plane curves corresponding to is exactly the same. According to (21), chaotic drive system can be reconstructed as $\xi = \xi(t) = (\eta_1^I, \eta_2^I, \eta_1^{VI}, \eta_2^{VI})$. Fig. 3 presents the project curves of the reconstructed system.Compared Fig. 1 with Fig. 3, we can find out that not only the shape, but also the position of the project curves of the reconstructed system are almost the same with the chaotic drive system (22). Therefore, it can be concluded that the state of reconstructed chaotic drive system and the state of the chaotic drive system is identical. Fig. 4 (a) presents the each state error between the reconstructed system and chaotic drive system (22).

As we can see that each state error between the drive system and reconstructed drive system can nearly be ignored. Where e_1, e_2, e_3, e_4 are defined as $e_1 = x_1 - \eta_1^I$, $e_2 = x_2 - \eta_2^I$, $e_3 = x_3 - \eta_1^{VI}$, $e_4 = x_4 - \eta_2^{VI}$. This verifies the corollary that the state of the reconstructed system and the state of the drive system (22) is exactly the same Fig. 4 (b) presents a contract of the result of this paper and the result of reference [79]. Under the same circumstance, blue line represent the total error of the method proposed in this paper while the red line represent the total state error of the paper [79].

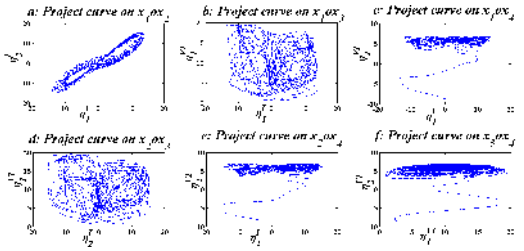

FIGURE 3. Projections of the reconstructed system.

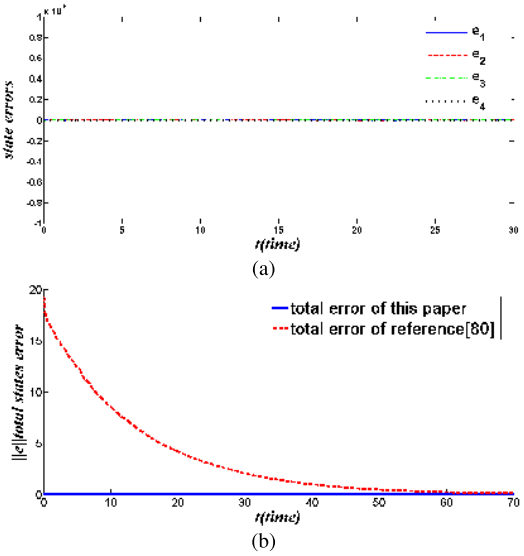

FIGURE 4. State errors of the proposed method. (a) The error between the drive system and reconstructed system, (b) The total state error between this paper and ref [79].

Total state error is defined as $\|e\| = \sqrt{e_1^2 + e_2^2 + e_3^2 + e_4^2}$. In paper [79], the adaptive control method was applied. The state error asymptotically converge to zero, it implies that the bigger the initial difference is, the longer it takes to converge to zero. Whereas, the total error of method proposed in this paper can be nearly ignored and is unacted on the difference between the initial state of the drive and response system. Due to a series of rotation and translation, the state of the drive system and response system is completely the same. So from this point of view, our method precede the method proposed in paper [79].

VI. IMAGE ENCRYPTION SCHEME

Image encryption algorithm has made great progress with the improvement of computer computing power, because image encryption often costs more and more with the improvement of encryption algorithm complexity(Refs. [80]–[83]). In this paper, a lightweight image encryption algorithm based on shape synchronization is proposed.

A. THE FLOW CHART OF ALGORITHM DESIGN (FIG.5)

In order to design a kind of image encryption algorithm based on 4-D chaotic system, it is necessary to ensure the security of the key during the color image transmission under the circumstance that the encryption effect is good. Therefore,

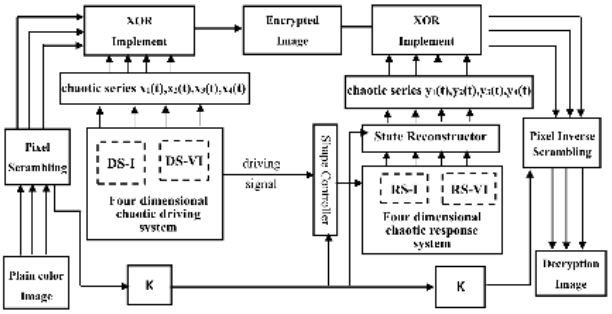

FIGURE 5. The flow chart of algorithm design.

the chaos shape synchronization theory is used. Senders use image scrambling algorithm of Baker's map firstly, then XOR operation with the chaotic sequence generated by the driving chaotic system, send enciphered image, key and driving signal during transmission. When the recipient gets the file, he uses the shape controller to synchronize the response system in shape firstly, then State Reconstructor component to reach complete synchronization, decrypts it through the inverse operation to obtain the decryption image at last.

B. DESIGN FOR IMAGE ENCRYPTION ALGORITHM

The detailed encryption steps are described as:

Step 1: Assume the color plain image P with the size $M \times N$, split P into its R, G, B component and obtain 3 grayscale image matrices, each size is $M \times N$. Then, expend the size of the obtained grayscale image matrices to $n \times n$ with 0, and denote the expended matrices as OR, OG and OB respectively, where $n = max\{M, N\}$.

Step 2: Using the Baker's map [84] to scramble the matrices OR, OG and OB. After different rounds of scrambling on three component, reshape the scrambled matrices into three vectors and denoted as DR, DG, DB respectively.

Step 3: Using the 4-D chaotic sequence to generate a four dimensional chaotic sequence, and truncate a chaotic sequence $x(k) \in R^{4\times(n\times n)}$of length $n \times n$ from r position. Then, generate four integer sequences of $X_i \in [0, 256]$ by Eq. (26).

$$X_i = mod(floor(x_i(k) \times 10^7), 256), \quad i = 1, 2, 3, 4; \quad (26)$$

At the same time, the initial tangent vector and normal vector $T_{12}^0, N_{12}^0, T_{34}^0, N_{34}^0$ of the projection curve of the chaotic attractor are calculate, which are saved as a part of Key.

Step 4: Employing the chaotic sequence to mask the scrambled pixels DR, DG, DB. The ciphered image $C = (C_r(i), C_g(i), C_b(i))$ is obtained according Eq. (27).

$$\begin{cases} C_r(i) = DR(i) \oplus X_1(i) \oplus X_2(i), & i = 1, 2, \ldots n^2 \\ C_g(i) = DG(i) \oplus X_2(i) \oplus X_3(i), & i = 1, 2, \ldots n^2 \\ C_b(i) = DB(i) \oplus X_3(i) \oplus X_4(i), & i = 1, 2, \ldots n^2 \end{cases} \quad (27)$$

Key$= [x_0, \theta_R, \theta_G, \theta_B, r, T_{12}^0, N_{12}^0, T_{34}^0, N_{34}^0]$

Remark 5: x_0 denotes the initial value of drive system, θ_R, θ_G, θ_B denote the rounds of scrambling on the three components of original color image, r denotes the start position of extracted the chaotic sequence. T_{12}^0, N_{12}^0 denote the initial point tangent vector and normal vector of DS-I system(the projective system of drive system on x_1ox_2). T_{34}^0, N_{34}^0 denote the initial point tangent vector and normal vector of $DS - VI$ system (the projective system of drive system on x_3ox_4).

C. DESIGN FOR IMAGE DECRYPTION ALGORITHM

The detailed decryption steps are described as:

Step 1: Under the effect of the shape synchronization controller, response system and chaotic drive system will achieve shape synchronization. The state of the response system is not exactly the same as the state of the drive system even though shape synchronization has been achieved. Using K $(x_0, \theta_R, \theta_G, \theta_B, T_{12}^0, N_{12}^0, T_{34}^0, N_{34}^0)$, the state constructor then generate complete synchronized chaotic signal.

Step 2: Use the same step of 3 of encryption algorithm, get sequence signal y_1, y_2, y_3, y_4.

Step 3: Decrypt the ciphered image $C = (C_r(i), C_g(i), C_b(i))$ as shown in Eq. (28), to get the $\widehat{DR}, \widehat{DG}, \widehat{DB}$ without chaotic signal.

$$\begin{cases} \widehat{DR} = C_r(i) \oplus Y_1(i) \oplus Y_2(i), & i = 1, 2 \ldots .n^2 \\ \widehat{DG} = C_g(i) \oplus Y_2(i) \oplus Y_3(i), & i = 1, 2 \ldots .n^2 \\ \widehat{DB} = C_b(i) \oplus Y_3(i) \oplus Y_4(i), & i = 1, 2 \ldots .n^2 \end{cases} \quad (28)$$

Step 4: Use the same step of 2 of encryption algorithm to get the recovered image.

D. EXPERIMENTAL RESULTS AND ANALYSIS

In the encryption process, this paper selects 512×512 Lena image (Fig. 6 (a)), $M = N = n = 512$. Then according to the shape synchronization of response system, the image can be decrypted (Fig. 6 (b)). The three component image of original plain color image and encrypted image are shown below (Fig. 6 (c)- (h)). We also chose two special images (all white and all black) to be encrypted and the results are shown in Fig. 7 (a)-(d).

1) HISTOGRAM ANALYSIS

The histogram is used to describe the distribution with respect to pixel values in their finite field. The distribution of the plain color image is usually steep, thus, the obvious features can easily obtained by hackers. As a good encryption algorithm, the ideal histogram of a encrypted should be uniformly distributed to prevent the attacker from any statistical information. Fig. 8 (a), (b), (c) show the histograms three component of the plain color images, and Fig. 8 (d), (e), (f) show their respective encrypted images. It is clear from Fig. 8 that the histograms of the cipher images are fairly uniform and significantly different from the histograms of the plain color images. Variances of histograms are listed in Table 4. The lower value of variances indicates the higher uniformity of ciphered images. In Table 4, the variance value is 1007039.1216 for histogram for histogram of B channel of the plain image Lena,which is greater than the variance 930.7373 for histogram of B channel of ciphered image Lena

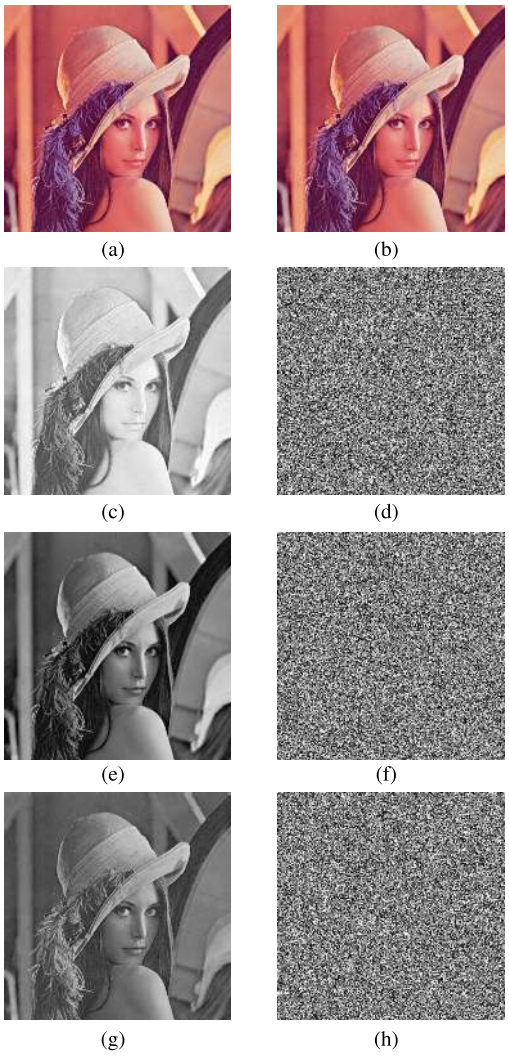

FIGURE 6. Encryption and encryption of images. (a) Original color image of Lena,(b) Decrypted color image of Lena, (c) R path of original color image, (d) R path of encrypted color image, (e) G path of original color image, (f) G path of encrypted color image, (g) B path of original color image, (h) B path of encrypted color image.

TABLE 4. Variances of histograms compared the plain-images and ciphered images.

Image	Plain Image	Ciphered image
Color Lena(R)	1007039.1216	1193.7569
Color Lena(G)	1007039.1216	1063.9608
Color Lena(B)	1007039.1216	930.7373

using the proposed algorithm. Therefore, the proposed algorithm is efficient.

2) CORRELATION ANALYSIS OF ADJACENT PIXEL

It is known a pixel in an image is highly correlated to its neighborhoods, and hackers can recover the plain color image through analyzing the correlation information. Therefore, the correlation between the adjacent pixels of the encrypted image is an important index to characterize the quality of an image encryption algorithm. The correlation coefficients r_{xy}

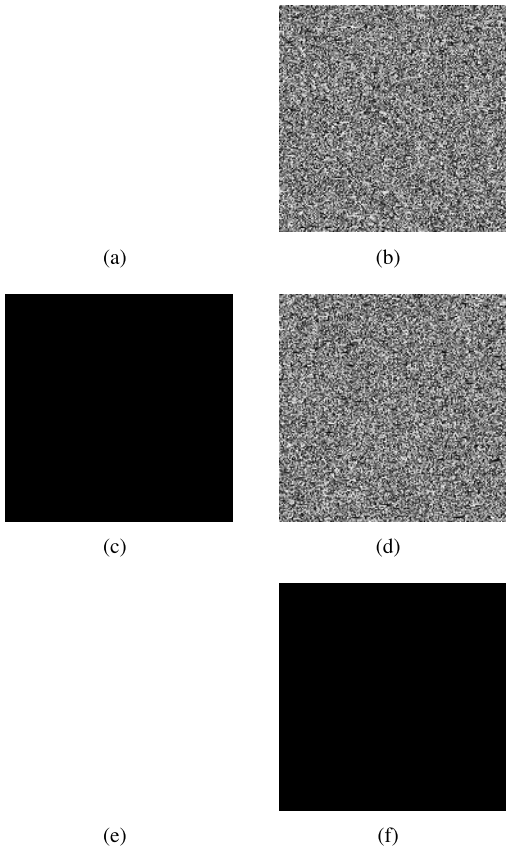

FIGURE 7. Encryption and decryption of white and black images. (a) Original image of White, (b) Encrypted image of White, (c) Original image of Black, (d) Encrypted image of Black, (e) Decrypted image of White, (f) Decrypted image of Black.

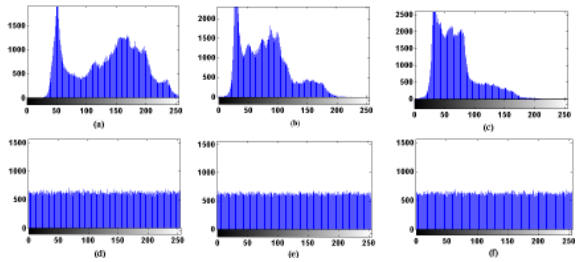

FIGURE 8. Histogram of plain color image and ciphered image. (a) Histogram of R channel of color Lena, (b) Histogram of G channel of color Lena, (c) Histogram of B channel of color Lena, (d) Histogram of R channel of ciphered color Lena image, (e) Histogram of G channel of ciphered color Lena image, (f) Histogram of B channel of ciphered color Lena image.

of two adjacent pixels can be computed by Eq. (29)

$$r_{xy} = \frac{cov(x, y)}{\sqrt{D(x)D(y)}} \tag{29}$$

in which $cov(x, y) = \frac{1}{N}\sum_{i=1}^{N}((x_i - E(x))(y_i - E(y)))$. $E(x) = \frac{1}{N}\sum_{i=1}^{N} x_i$ and $D(x) = \frac{1}{N}\sum_{i=1}^{N}(x_i - E(x))^2$ are the expectation and variance of variable x, respectively. N denotes the number of pixels obtained from the image. 5000 pairs of adjacent pixels from the original images and the cipher images are randomly chosen and the pixel correlations results in three directions are illustrated in Table 5. It is clear that the correlation of the encrypted image is effectively removed and

TABLE 5. Correlation coefficients of adjacent pixels.

Correlation	Horizontal	Vertical	Diagonal
Plain image (Fig. 6 (a))	0.9819	0.9715	0.9560
Encrypted image (Fig. 6 (b))	0.0023	0.0049	0.0153

TABLE 6. Correlation coefficients.

Result comparison	R	G	B
Fig. 6 (a)	7.2722	7.5855	7.0100
Fig. 6 (b)	7.9993	7.9993	7.9993
Lena in(Ref. [85])	7.991362	7.991499	7.991603
Lena in(Ref. [86])	7.9893	7.9896	7.9903
Lena in(Ref. [87])	7.9974	7.9974	7.9974
Lena in(Ref. [88])	7.989825	7.989120	7.990007

the correlation coefficients are close to zero, which means the algorithm is very effective.

3) INFORMATION ENTROPY ANALYSIS

Information entropy can be used to characterize the richness of information. The information entropy values for some plain color images and encrypted images using the proposed algorithm have been calculated and illustrated in Table 6. From these results, we can watch that the information entropy values of all encrypted images are very near 8, and the encrypted images generated by our algorithm have better random distributions, and the information leakage is negligible.

VII. CONCLUSION

Today, with the application of more and more widely varied information transmission on the Internet, information encryption technology has played a very important role. So in this paper, we used the 4-D chaotic systems,then designed the shape controllers to make synchronization between different chaotic and dimensions systems in shape. Finally a lightweight image encryption was put into practice and final simulation experiments carried out. In this paper,the use of shape synchronization theory in the field of image encryption, to ensure that the encryption is effectiveness and practicability. But the decryption of the image does not appear to be a defect of the phenomenon. In the future work, we need to further study the safety of the algorithm.

REFERENCES

[1] K. Gu, N. Wu, B. Yin, and W. Jia, "Secure data sequence query framework based on multiple fogs," *IEEE Trans. Emerg. Topics Comput.*, early access, Sep. 24, 2019, doi: 10.1109/TETC.2019.2943524.

[2] Z. Liao, J. Peng, Y. Chen, J. Zhang, and J. Wang, "A fast Q-Learning based data storage optimization for low latency in data center networks," *IEEE Access*, vol. 8, pp. 90630–90639, 2020.

[3] K. Gu, N. Wu, B. Yin, and W. Jia, "Secure data query framework for cloud and fog computing," *IEEE Trans. Netw. Service Manage.*, vol. 17, no. 1, pp. 332–345, Mar. 2020.

[4] Z. Xia, Z. Fang, F. Zou, J. Wang, and A. K. Sangaiah, "Research on defensive strategy of real-time price attack based on multiperson zero-determinant," *Secur. Commun. Netw.*, vol. 2019, Jul. 2019, Art. no. 6956072.

[5] K. Gu, W. Zhang, S.-J. Lim, P. K. Sharma, Z. Al-Makhadmeh, and A. Tolba, "Reusable mesh signature scheme for protecting identity privacy of IoT devices," *Sensors*, vol. 20, no. 3, p. 758, Jan. 2020.

[6] K. Gu, X. Dong, and L. Wang, "Efficient traceable ring signature scheme without pairings," *Adv. Math. Commun.*, vol. 14, no. 2, pp. 207–232, 2020.

[7] Z. Hua, Y. Zhang, and Y. Zhou, "Two-dimensional modular chaotification system for improving chaos complexity," *IEEE Trans. Signal Process.*, vol. 68, pp. 1937–1949, 2020.

[8] F. Yu, L. Liu, H. Shen, Z. Zhang, Y. Huang, S. Cai, Z. Deng, and Q. Wan, "Multistability analysis, coexisting multiple attractors and FPGA implementation of Yu-Wang four-wing chaotic system," *Math. Problems Eng.*, vol. 2020, Aug. 2020, Art. no. 7530976.

[9] F. Yu, L. Liu, L. Xiao, K. Li, and S. Cai, "A robust and fixed-time zeroing neural dynamics for computing time-variant nonlinear equation using a novel nonlinear activation function," *Neurocomputing*, vol. 350, no. 20, pp. 108–116, Jul. 2019.

[10] J. Jin, L. Zhao, M. Li, F. Yu, and Z. Xi, "Improved zeroing neural networks for finite time solving nonlinear equations," *Neural Comput. Appl.*, vol. 32, no. 9, pp. 4151–4160, May 2020.

[11] L. Zhou, F. Tan, F. Yu, and W. Liu, "Cluster synchronization of two-layer nonlinearly coupled multiplex networks with multi-links and time-delays," *Neurocomputing*, vol. 359, pp. 264–275, Sep. 2019.

[12] H. Lin, C. Wang, and Y. Tan, "Hidden extreme multistability with hyperchaos and transient chaos in a Hopfield neural network affected by electromagnetic radiation," *Nonlinear Dyn.*, vol. 99, no. 3, pp. 2369–2386, Feb. 2020.

[13] F. Wang, L. Zhang, S. Zhou, and Y. Huang, "Neural network-based finite-time control of quantized stochastic nonlinear systems," *Neurocomputing*, vol. 362, no. 14, pp. 195–202, Oct. 2019.

[14] C. Wang, L. Xiong, J. Sun, and W. Yao, "Memristor-based neural networks with weight simultaneous perturbation training," *Nonlinear Dyn.*, vol. 95, no. 4, pp. 2893–2906, Mar. 2019.

[15] W. Yao, C. Wang, J. Cao, Y. Sun, and C. Zhou, "Hybrid multisynchronization of coupled multistable memristive neural networks with time delays," *Neurocomputing*, vol. 363, pp. 281–294, Oct. 2019.

[16] C. Zhou, C. Wang, Y. Sun, and W. Yao, "Weighted sum synchronization of memristive coupled neural networks," *Neurocomputing*, vol. 403, pp. 225–232, Aug. 2020.

[17] Y. Tan and C. Wang, "A simple locally active memristor and its application in HR neurons," *Chaos, Interdiscipl. J. Nonlinear Sci.*, vol. 30, no. 5, May 2020, Art. no. 053118.

[18] J. Sun, X. Zhao, J. Fang, and Y. Wang, "Autonomous memristor chaotic systems of infinite chaotic attractors and circuitry realization," *Nonlinear Dyn.*, vol. 94, no. 4, pp. 2879–2887, Dec. 2018.

[19] J. Sun, G. Han, Z. Zeng, and Y. Wang, "Memristor-based neural network circuit of full-function pavlov associative memory with time delay and variable learning rate," *IEEE Trans. Cybern.*, early access, Nov. 21, 2019, doi: 10.1109/TCYB.2019.2951520.

[20] F. Yu, Q. Wan, J. Jin, L. Li, B. He, L. Liu, S. Qian, Y. Huang, S. Cai, Y. Song, and Q. Tang, "Design and FPGA implementation of a pseudo-random number generator based on a four-wing memristive hyperchaotic system and Bernoulli map," *IEEE Access*, vol. 7, pp. 181884–181898, 2019.

[21] F. Yu, L. Li, Q. Tang, S. Cai, Y. Song, and Q. Xu, "A survey on true random number generators based on chaos," *Discrete Dyn. Nature Soc.*, vol. 2019, Dec. 2019, Art. no. 2545123.

[22] L. Zhou, F. Tan, and F. Yu, "A robust synchronization-based chaotic secure communication scheme with double-layered and multiple hybrid networks," *IEEE Syst. J.*, vol. 14, no. 2, pp. 2508–2519, Jun. 2020.

[23] F. Yu, S. Qian, X. Chen, Y. Huang, L. Liu, C. Shi, S. Cai, Y. Song, and C. Wang, "A new 4D four-wing memristive hyperchaotic system: Dynamical analysis, electronic circuit design, shape synchronization and secure communication application," *Int. J. Bifurcation Chaos*, 2020. [Online]. Available: https://scholar.google.com/scholar?q=A+New+4D+FourWing+Memristive+Hyperchaotic+System:+Dynamical+Analysis,+Electronic+Circuit+Design,+Shape+Synchronization+and+Secure+Communication&hl=zh-CN&as_sdt=0,5, doi: 10.1142/S0218127420501412.

[24] F. Yu, L. Liu, B. He, Y. Huang, C. Shi, S. Cai, Y. Song, S. Du, and Q. Wan, "Analysis and FPGA realization of a novel 5D hyperchaotic four-wing memristive system, active control synchronization, and secure communication application," *Complexity*, vol. 2019, Nov. 2019, Art. no. 4047957.

[25] F. Yu, L. Liu, S. Qian, L. Li, Y. Huang, C. Shi, S. Cai, X. Wu, S. Du, and Q. Wan, "Chaos-based application of a novel multistable 5D memristive hyperchaotic system with coexisting multiple attractors," *Complexity*, vol. 2020, Mar. 2020, Art. no. 8034196.

[26] Y. He, Y.-Q. Zhang, and X.-Y. Wang, "A new image encryption algorithm based on two-dimensional spatiotemporal chaotic system," *Neural Comput. Appl.*, vol. 32, no. 1, Jan. 2020, Art. no. 106040.
[27] A. Laucka, D. Andriukaitis, A. Valinevicius, D. Navikas, M. Zilys, V. Markevicius, D. Klimenta, R. Sotner, and J. Jerabek, "Method for volume of irregular shape pellets estimation using 2D imaging measurement," *Appl. Sci.*, vol. 10, no. 8, p. 2650, Apr. 2020.
[28] M. Zhou and C. Wang, "A novel image encryption scheme based on conservative hyperchaotic system and closed-loop diffusion between blocks," *Signal Process.*, vol. 171, Jun. 2020, Art. no. 107484.
[29] S. Wang, C. Wang, and C. Xu, "An image encryption algorithm based on a hidden attractor chaos system and the Knuth–Durstenfeld algorithm," *Opt. Lasers Eng.*, vol. 128, May 2020, Art. no. 105995.
[30] C. Xu, J. Sun, and C. Wang, "An image encryption algorithm based on random walk and hyperchaotic systems," *Int. J. Bifurcation Chaos*, vol. 30, no. 4, Mar. 2020, Art. no. 2050060.
[31] Y.-Q. Zhang and X.-Y. Wang, "A symmetric image encryption algorithm based on mixed linear–nonlinear coupled map lattice," *Inf. Sci.*, vol. 273, pp. 329–351, Jul. 2014.
[32] Y.-Q. Zhang, J.-L. Hao, and X.-Y. Wang, "An efficient image encryption scheme based on S-boxes and fractional-order differential logistic map," *IEEE Access*, vol. 8, pp. 54175–54188, 2020.
[33] X. Wang and S. Gao, "Image encryption algorithm for synchronously updating Boolean networks based on matrix semi-tensor product theory," *Inf. Sci.*, vol. 507, pp. 16–36, Jan. 2020.
[34] H. Liu and X. Wang, "Color image encryption based on one-time keys and robust chaotic maps," *Comput. Math. Appl.*, vol. 77, pp. 6883–6896, Jan. 2018.
[35] X. Wang, L. Liu, and Y. Zhang, "A novel chaotic block image encryption algorithm based on dynamic random growth technique," *Opt. Lasers Eng.*, vol. 66, pp. 16–18, Mar. 2015.
[36] H. Liu and X. Wang, "Color image encryption using spatial bit-level permutation and high-dimension chaotic system," *Opt. Commun.*, vol. 284, nos. 16–17, pp. 3895–3903, Aug. 2011.
[37] Y.-Q. Zhang, Y. He, P. Li, and X.-Y. Wang, "A new color image encryption scheme based on 2DNLCML system and genetic operations," *Opt. Lasers Eng.*, vol. 128, May 2020, Art. no. 106040.
[38] X.-Y. Wang, P. Li, Y.-Q. Zhang, L.-Y. Liu, H. Zhang, and X. Wang, "A novel color image encryption scheme using DNA permutation based on the Lorenz system," *Multimedia Tools Appl.*, vol. 77, no. 5, pp. 6243–6265, Mar. 2018.
[39] H. Liu, X. Wang, and A. Kadir, "Image encryption using DNA complementary rule and chaotic maps," *Appl. Soft Comput.*, vol. 12, no. 5, pp. 1457–1466, May 2012.
[40] X.-Y. Wang, Y.-Q. Zhang, and X.-M. Bao, "A novel chaotic image encryption scheme using DNA sequence operations," *Opt. Lasers Eng.*, vol. 73, pp. 53–61, Oct. 2015.
[41] H. Wang, H.-F. Liang, and Z.-H. Miao, "A new color image encryption scheme based on chaos synchronization of time-delay Lorenz system," *Adv. Manuf.*, vol. 4, no. 4, pp. 348–354, Dec. 2016.
[42] S. Vaidyanathan, A. Akgul, S. Kaçar, and U. Çavusoglu, "A new 4-D chaotic hyperjerk system, its synchronization, circuit design and applications in RNG, image encryption and chaos-based steganography," *Eur. Phys. J. Plus*, vol. 133, no. 2, pp. 46–64, 2018.
[43] P. Muthukumar, P. Balasubramaniam, and K. Ratnavelu, "Sliding mode control design for synchronization of fractional order chaotic systems and its application to a new cryptosystem," *Int. J. Dyn. Control*, vol. 5, no. 1, pp. 115–123, Mar. 2017.
[44] P. Muthukumar, P. Balasubramaniam, and K. Ratnavelu, "Fast projective synchronization of fractional order chaotic and reverse chaotic systems with its application to an affine cipher using date of birth (DOB)," *Nonlinear Dyn.*, vol. 80, no. 4, pp. 1883–1897, Jun. 2015.
[45] E. Ott, C. Grebogi, and J. A. Yorke, "Controlling chaos," *Phys. Rev. Lett.*, vol. 64, pp. 1196–1199, Mar. 1990.
[46] L. M. Pecora and T. L. Carroll, "Synchronization in chaotic systems," *Phys. Rev. Lett.*, vol. 64, no. 8, pp. 21–824, 1990.
[47] L. Luan Ling and L.-J. Feng, "Synchronization of Bragg acousto-optic bistable system by active-passive method," *Acta Photonica Sinica*, vol. 39, no. 3, pp. 409–411, 2010.
[48] S. K. Agrawal, M. Srivastava, and S. Das, "Synchronization of fractional order chaotic systems using active control method," *Chaos, Solitons Fractals*, vol. 45, no. 6, pp. 737–752, Jun. 2012.
[49] M. Sun, Q. Jia, and L. Tian, "A new four-dimensional energy resources system and its linear feedback control," *Chaos, Solitons Fractals*, vol. 39, no. 1, pp. 101–108, Jan. 2009.
[50] C. Ge, C. Hua, and X. Guan, "Master–slave synchronization criteria of Lur'e systems with time-delay feedback control," *Appl. Math. Comput.*, vol. 24, pp. 895–902, Oct. 2012.
[51] Y. Li, W. K. S. Tang, and G. Chen, "Generating hyperchaos via state feedback control," *Int. J. Bifurcation Chaos*, vol. 15, no. 10, pp. 3367–3375, Oct. 2005.
[52] S. Mobayen and F. Tchier, "Synchronization of a class of uncertain chaotic systems with Lipschitz nonlinearities using state-feedback control design: A matrix inequality approach," *Asian J. Control*, vol. 20, no. 1, pp. 71–85, Jan. 2018.
[53] S. Mobayen and J. Ma, "Robust finite-time composite nonlinear feedback control for synchronization of uncertain chaotic systems with nonlinearity and time-delay," *Chaos, Solitons Fractals*, vol. 114, pp. 46–54, Sep. 2018.
[54] F. Wang, B. Chen, Y. Sun, Y. Gao, and C. Lin, "Finite-time fuzzy control of stochastic nonlinear systems," *IEEE Trans. Cybern.*, vol. 50, no. 6, pp. 2617–2626, Jun. 2020.
[55] X. Lv, X. Li, J. Cao, and M. Perc, "Dynamical and static multisynchronization of coupled multistable neural networks via impulsive control," *IEEE Trans. Neural Netw. Learn. Syst.*, vol. 29, no. 12, pp. 6062–6072, Dec. 2018.
[56] J. Sun, Y. Wang, Y. Wang, and Y. Shen, "Finite-time synchronization between two complex-variable chaotic systems with unknown parameters via nonsingular terminal sliding mode control," *Nonlinear Dyn.*, vol. 85, no. 2, pp. 1105–1117, Jul. 2016.
[57] J. Sun, Y. Wu, G. Cui, and Y. Wang, "Finite-time real combination synchronization of three complex-variable chaotic systems with unknown parameters via sliding mode control," *Nonlinear Dyn.*, vol. 88, no. 3, pp. 1677–1690, May 2017.
[58] M. Wang, L. Huang, and C. Yang, "NN-based adaptive tracking control of discrete-time nonlinear systems with actuator saturation and event-triggering protocol," *IEEE Trans. Syst., Man, Cybern., Syst.*, early access, Apr. 9, 2020, doi: 10.1109/TSMC.2020.2981954.
[59] X. Xi, S. Mobayen, H. Ren, and S. Jafari, "Robust finite-time synchronization of a class of chaotic systems via adaptive global sliding mode control," *J. Vibrat. Control*, vol. 24, no. 17, pp. 3842–3854, Sep. 2018.
[60] F. Wang and X. Zhang, "Adaptive finite time control of nonlinear systems under time-varying actuator failures," *IEEE Trans. Syst., Man, Cybern., Syst.*, vol. 49, no. 9, pp. 1845–1852, Sep. 2019.
[61] G. M. Mahmoud and E. E. Mahmoud, "Complete synchronization of chaotic complex nonlinear systems with uncertain parameters," *Nonlinear Dyn.*, vol. 62, no. 4, pp. 875–882, Dec. 2010.
[62] H. Li, X. Liao, and M. Luo, "A novel non-equilibrium fractional-order chaotic system and its complete synchronization by circuit implementation," *Nonlinear Dyn.*, vol. 68, nos. 1–2, pp. 137–149, Apr. 2012.
[63] X.-J. Wu and H.-T. Lu, "Generalized projective lag synchronization between different hyperchaotic systems with uncertain parameters," *Nonlinear Dyn.*, vol. 66, nos. 1–2, pp. 185–200, Oct. 2011.
[64] G. Peng and Y. Jiang, "Generalized projective synchronization of a class of fractional-order chaotic systems via a scalar transmitted signal," *Phys. Lett. A*, vol. 372, no. 22, pp. 3963–3970, May 2008.
[65] A. Khan and M. A. Bhat, "Hyperchaotic analysis and adaptive projective synchronization of nonlinear dynamical system," *Comput. Math. Model.*, vol. 28, no. 4, pp. 517–530, Oct. 2017.
[66] J. Meng and X.-Y. Wang, "Nonlinear observer based phase synchronization of chaotic systems," *Phys. Lett. A*, vol. 369, no. 4, pp. 294–298, Sep. 2007.
[67] M. Hasler, Y. Maistrenko, and O. Popovych, "Simple example of partial synchronization of chaotic systems," *Phys. Rev. E, Stat. Phys. Plasmas Fluids Relat. Interdiscip. Top.*, vol. 58, no. 5, pp. 6843–6846, Nov. 1998.
[68] N. F. Rulkov, M. M. Sushchik, L. S. Tsimring, and H. D. I. Abarbanel, "Generalized synchronization of chaos in directionally coupled chaotic systems," *Phys. Rev. E, Stat. Phys. Plasmas Fluids Relat. Interdiscip. Top.*, vol. 980, no. 51, pp. 598–608, 1995.
[69] S. Hammami, M. Benrejeb, M. Feki, and P. Borne, "Feedback control design for Rössler and Chen chaotic systems anti-synchronization," *Phys. Lett. A*, vol. 374, no. 28, pp. 2835–2840, Jun. 2010.
[70] L. Ren, R. Guo, and U. E. Vincent, "Coexistence of synchronization and anti-synchronization in chaotic systems," *Arch. Control Sci.*, vol. 26, no. 1, pp. 69–79, Mar. 2016.
[71] Y.-Y. Huang, Y.-H. Wang, and Y. Zhang, "Shape synchronization of drive-response for a class of two-dimensional chaotic systems via continuous controllers," *Nonlinear Dyn.*, vol. 78, no. 4, pp. 2331–2340, Dec. 2014.

[72] Y. Huang, Y. Wang, H. Chen, and S. Zhang, "Shape synchronization control for three-dimensional chaotic systems," *Chaos, Solitons Fractals*, vol. 87, pp. 136–145, Jun. 2016.
[73] A. Chen, J. Lu, J. Lü, and S. Yu, "Generating hyperchaotic Lü attractor via state feedback control," *Phys. A, Stat. Mech. Appl.*, vol. 364, pp. 103–110, May 2016.
[74] X. Wang and M. Wang, "A hyperchaos generated from Lorenz system," *Phys. A, Stat. Mech. Appl.*, vol. 387, no. 14, pp. 3751–3758, Jun. 2008.
[75] F. Yu, H. Shen, L. Liu, Z. Zhang, Y. Huang, B. He, S. Cai, Y. Song, B. Yin, S. Du, and Q. Xu, "CCII and FPGA realization: A multistable modified fourth-order autonomous Chua's chaotic system with coexisting multiple attractors," *Complexity*, vol. 2020, Mar. 2020, Art. no. 5212601.
[76] F. Yu, L. Liu, H. Shen, Z. Zhang, Y. Huang, C. Shi, S. Cai, X. Wu, S. Du, and Q. Wan, "Dynamic analysis, circuit design, and synchronization of a novel 6D memristive four-wing hyperchaotic system with multiple coexisting attractors," *Complexity*, vol. 2020, May 2020, Art. no. 5904607.
[77] M. P. D. Carmo, *Differential Geometry of Curves and Surfaces*. Englewood Cliffs, NJ, USA: Prentice-Hall, 1976.
[78] S. S. Chern, *Lectures on Differential Geometry*. Singapore: World Scientific, 1999.
[79] C. Xu, J.-W. Feng, F. Austin, and W.-Q. Zhang, "Adaptive synchronization between hyperchaotic Lorenz system and Chen system," in *Proc. Int. Conf. Comput. Intell. Secur.*, Beijing, China, vol. 1, 2009, pp. 662–665.
[80] Y. Chen, W. Xu, J. Zuo, and K. Yang, "The fire recognition algorithm using dynamic feature fusion and IV-SVM classifier," *Cluster Comput.*, vol. 22, pp. 7665–7675, May 2018.
[81] D. Zhang, T. Yin, G. Yang, M. Xia, L. Li, and X. Sun, "Detecting image seam carving with low scaling ratio using multi-scale spatial and spectral entropies," *J. Vis. Commun. Image Represent.*, vol. 48, pp. 281–291, Oct. 2017.
[82] M. Long, F. Peng, and Y. Zhu, "Identifying natural images and computer generated graphics based on binary similarity measures of PRNU," *Multimedia Tools Appl.*, vol. 78, no. 1, pp. 489–506, Jan. 2019.
[83] D. Zhang, Z. Liang, G. Yang, Q. Li, L. Li, and X. Sun, "A robust forgery detection algorithm for object removal by exemplar-based image inpainting," *Multimedia Tools Appl.*, vol. 77, no. 10, pp. 11823–11842, May 2018.
[84] I. Hussain and M. A. Gondal, "Stego Optical Encryption Based on Chaotic Baker's Map Transformation," *Opt. Laser Technol.*, vol. 61, nos. 5–6, pp. 50–56, 2014.
[85] A. Kadir, M. Aili, and M. Sattar, "Color image encryption scheme using coupled hyper chaotic system with multiple impulse injections," *Optik-Int. J. Light Electron Opt.*, vol. 129, pp. 231–238, Jan. 2017.
[86] X. Wu, H. Kan, and J. Kurths, "A new color image encryption scheme based on DNA sequences and multiple improved 1D chaotic maps," *Appl. Soft Comput.*, vol. 37, pp. 24–39, Dec. 2015.
[87] X. Wang, S. Wang, Y. Zhang, and C. Luo, "A one-time pad color image cryptosystem based on SHA-3 and multiple chaotic systems," *Opt. Lasers Eng.*, vol. 103, pp. 1–8, Apr. 2018.
[88] H. Liu, Y. Zhang, A. Kadir, and Y. Xu, "Image encryption using complex hyper chaotic system by injecting impulse into parameters," *Appl. Math. Comput.*, vol. 360, pp. 83–93, Nov. 2019.

YUANYUAN HUANG was born in Longhui, Hunan, China, in 1979. She received the B.E. degree from the University of South China, Hengyang, in 2002, the M.E. degree from Hunan Normal University, Changsha, China, in 2005, and the Ph.D. degree from the Guangdong University of Technology, Guangzhou, in 2015. She is currently a Lecturer with the School of Computer and Communication Engineering, Changsha University of Science and Technology, Changsha. Her research interests include nonlinear control, complex systems, adaptive fuzzy control, and chaos synchronization control and its application.

LONGWANG HUANG received the B.Sc. degree in automation engineering from the Jiangxi University of Science and Technology, Ganzhou, China, in 2015, and the M.Sc. degree in control science and engineering from the Guangdong University of Technology, Guangzhou, in 2018. He is currently pursuing the Ph.D. degree with the South China University of Technology. His research interests include nonlinear control, adaptive neural network control, learning control, control of the networked systems, and chaotic system control.

YINHE WANG received the M.S. degree in mathematics from Sichuan Normal University, Chengdu, China, in 1990, and the Ph.D. degree in control theory and engineering from Northeastern University, Shenyang, China, in 1999. From 2000 to 2002, he held a postdoctoral position with the Department of Automatic Control, Northwestern Polytechnical University, Xi'an, China. From 2005 to 2006, he was a Visiting Scholar with the Department of Electrical Engineering, Lakehead University, Canada. He is currently a Professor with the School of Automation, Guangdong University of Technology, Guangzhou, China. His research interests include fuzzy adaptive robust control, analysis for nonlinear systems, and complex dynamical networks.

YUXU PENG received the B.E. degree from the Shandong University of Technology, Jinan, China, in 1999, the M.E. degree from the Changsha Jiaotong College, Changsha, China, in 2002, and the Ph.D. degree from the Nanjing University of Posts and Telecommunications, Nanjing, China, in 2007. He is currently an Associate Professor with the School of Computer and Communication Engineering, Changsha University of Science and Technology, Changsha. His research interests include protein shape retrieval, deep learning, and big data processing.

FEI YU was born in Anqing, Anhui, China, in 1984. He received the B.E. degree from Anhui Normal University, in 2007, and the M.E. and Ph.D. degrees from the College of Information Science and Engineering, Hunan University, Changsha, China, in 2010 and 2013, respectively. He is currently a Lecturer with the School of Computer and Communication Engineering, Changsha University of Science and Technology, Changsha. His research interests include radio frequency integrated circuits design, UWB antenna design, and chaos generation, synchronization, and its application.